JMEPEG (2016) 25:4408–4415
DOI: 10.1007/s11665-016-2294-y

1059-9495/$19.00

On the Influence of Material Parameters in a Complex Material Model for Powder Compaction

Hjalmar Staf, Per Lindskog, Daniel C. Andersson, and Per-Lennart Larsson

(Submitted February 12, 2016; in revised form August 3, 2016; published online August 26, 2016)

Parameters in a complex material model for powder compaction, based on a continuum mechanics approach, are evaluated using real insert geometries. The parameter sensitivity with respect to density and stress after compaction, pertinent to a wide range of geometries, is studied in order to investigate completeness and limitations of the material model. Finite element simulations with varied material parameters are used to build surrogate models for the sensitivity study. The conclusion from this analysis is that a simplification of the material model is relevant, especially for simple insert geometries. Parameters linked to anisotropy and the plastic strain evolution angle have a small impact on the final result.

Keywords constitutive model, material characterization, powder compaction, real inserts, sensitivity analysis

1. Introduction

Classic cutting inserts are manufactured by compacting hard metal powder blends into a predefined shape followed by sintering to full density and posttreatment. When designing a new cutting insert, the shape of the pressing tool is often an issue, since the density after compaction and therefore also the shrinkage during sintering is uneven and hard to predict. By making simulations of the manufacturing process based on the finite element (FE) method, the shape of an insert after compaction and sintering can be predicted and used for design of pressing tools (Ref 1).

Modeling of powder compaction can roughly by divided into two types, describing either pressing up to intermediate or up to high densities. The first type can be described as a micromechanical approach using analytical (Ref 2) or numerical methods, such as the discrete element method (DEM) (Ref 3-5). In (Ref 4, 5), DEM simulations are compared with experiments and it was concluded that the numerical results are accurate up to material densities being approximately 50–60% of a fully compacted insert, which evidently is not sufficient for simulation of the manufacturing process.

The reason for failure of the micromechanical models at higher densities is that such models are based on the mechanical behavior at particle-particle (powder-powder) contacts. Out of necessity, it is most often assumed that each powder contact is mechanically independent of the neighboring contacts. At higher densities, such an assumption is no longer accurate. It should be noted that research has been conducted in order to include the effect from neighboring contacts into micromechanical modeling of powder compaction (Ref 6, 7).

At the moment, however, DEM modeling at high densities is an undeveloped research field where large computer capacity is needed for simulation of whole insert geometries. Consequently, some type of macroscopic approach has to be relied upon in this situation in order to describe the powder compaction process completely in an accurate (and practical) manner.

In doing so, powder compaction to high density is mostly treated phenomenological assuming a porous solid and using, for example, a Gurson model (Ref 8), a CamClay model (Ref 9) or a Drucker-Prager CAP model (Ref 10). Here, a material model that can be described as an extended Drucker-Prager CAP model, suggested by (Ref 11), with material parameters presented in (Ref 12) is scrutinized. The model is complex with many material parameters, which makes it very hard to define a complete set of parameters for a specific powder blend. Previous research presented in (Ref 12) on inverse modeling with an instrumented die (Ref 13), where the force against a die wall and press forces was compared with FE-simulations, shows that either a less complex material model or more extensive tests, or a combination of both, are needed to complete a full material description including characterization. From this inverse modeling, it was possible to determine a limited number of material curves and material constants but not nearly sufficient for completely determining the constitutive behavior.

To better understand which parameters of the material model (Ref 11) could be possibly disregarded and to suggest further material characterization tests, sensitivity studies are presently performed. To some extent, this is performed in (Ref 14), but there is a need to do this for different kinds of stress fields, i.e., more inserts, and recording responses over the whole cutting insert. In this paper, FE-simulations of a number of real inserts with totally different geometries are used to perform sensitivity analysis for the material parameters. The response variables are density and stress, after compaction or at maximum compaction, at 10–20 points over the whole geometry.

2. Material Model

The material model used in this study, presented in (Ref 11) and used in (Ref 1), (Ref 12) and (Ref 13), is an elastic-plastic

Hjalmar Staf, Department of Solid Mechanics, Royal Institute of Technology, 10044 Stockholm, Sweden; and Sandvik Coromant AB, R&D, SE-12680, Stockholm, Sweden; **Per Lindskog**, Sandvik Coromant AB, R&D, 12680 Stockholm, Sweden; and **Daniel C. Andersson**, Inspecta Sweden AB, Box 30100, 10425 Stockholm, Sweden; **Per-Lennart Larsson**, Department of Solid Mechanics, Royal Institute of Technology, SE-10044, Stockholm, Sweden. Contact e-mail: plla@kth.se.

model with a yield surface of Drucker-Prager CAP kind. To determine the yield surface an elliptic cap part f^{CAP} and a quadratic failure curve f^{failure}, as a function of relative density d (density divided by sintered density), the first invariant of the Cauchy stress tensor σ_{I} and the second invariant of the deviatoric stress tensor σ_{II} are defined in Eq 1–5.

The function f^{CAP} and f^{failure} yields.

$$f^{\mathrm{CAP}}(d,\sigma_{\mathrm{I}},\sigma_{\mathrm{II}}) = \sqrt{\sigma_{\mathrm{II}}} - \frac{1}{R}\sqrt{(L-X(d))^2-(L-\sigma_{\mathrm{I}})^2} \quad \text{(Eq 1)}$$

$$f^{\mathrm{failure}}(d,\sigma_{\mathrm{I}},\sigma_{\mathrm{II}}) = \sqrt{\sigma_{\mathrm{II}}} - \left(c_0(d) - c_1(d)\sigma_{\mathrm{I}} + c_2(d)\sigma_{\mathrm{I}}^2\right) \quad \text{(Eq 2)}$$

where R, L, $X(d)$ and $Y(d)$ are material parameters and

$$c_0(d) = -Y(d)\frac{\frac{L^2}{\sqrt{3}} - \frac{L-X(d)}{R}(Y(d)-2L)}{L^2+Y(d)(Y(d)-2L)} \quad \text{(Eq 3)}$$

$$c_1(d) = 2Lc_2(d) \quad \text{(Eq 4)}$$

$$c_2(d) = -\frac{\frac{Y(d)}{\sqrt{3}} + \frac{L-X(d)}{R}}{L^2+Y(d)(Y(d)-2L)} \quad \text{(Eq 5)}$$

An offset φ from the associative flow direction is determined as a function of the proportion between deviatoric and volumetric stress J_φ defined by

$$J_\varphi = \frac{\sigma_{\mathrm{ii}}}{X(d)} \quad \text{(Eq 6)}$$

Further the material model accounts for anisotropy, described as the intensity of plastic anisotropy e and resulting in kinematic hardening. The back stress κ gives kinematic hardening by, in the yield function, replacing σ with σ- κ. A second-order stretch tensor P defined in (Ref 11) is coaxial with κ as shown in Eq 7, yielding the back stress

$$\kappa = h(e)\sigma_{\mathrm{I}}\frac{P'}{\sqrt{P'_{\mathrm{II}}}} \quad \text{(Eq 7)}$$

where P' and P'_{II} are the deviator and second invariant of P, respectively, h is a scaling function and e is updated based on the evolution of plastic shear strain, deviatoric plastic work and volumetric plastic work defined by the linear constants c_{a}, c_{d} and c_{v}.

The hyperelastic behavior is assumed to be isotropic and described with density dependent bulk modulus $K(d)$ and Poisson's ratio ν.

In summary, the material constants and functions are:

L and ***R*** are material constants that define the yield surface as shown in Fig. 1. L is related to hydrostatic compressive yield. Both are included in the sensitivity study with a small area of interest due to their high impact.

X(d), ***Y(d)*** and ***C(d)*** are hydrostatic compressive yield stress, uniaxial compressive yield stress and shear yield stress, all as a function of relative density d, shown in Fig. 2. In the sensitivity study, they are included by changing the magnitude of the curve with scale factors *CX*, *CY* and *CC,* respectively.

K(d) is the bulk modulus as a function of relative density d, shown in Fig. 2(a) and included in the sensitivity analysis with scale factor *CK*.

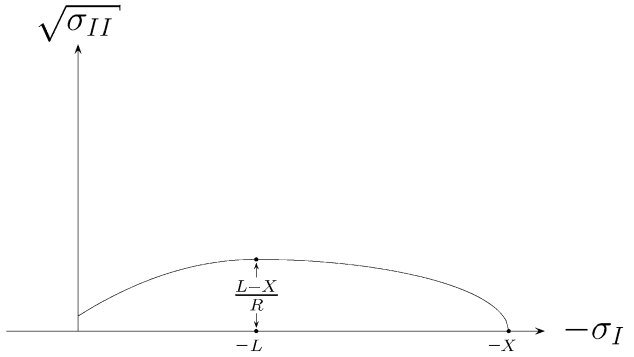

Fig. 1 Schematic of the yield surface in the material model (Ref 11) and used in analysis

φ(*d*) is the plastic strain evolution angle as a function of d, shown in Fig. 2(e) and included in the sensitivity analysis with scale factor *CFI*.

ν is Poisson's ratio and included in the sensitivity study as a variable *PR*.

$\boldsymbol{c_{\mathrm{a}}}$, $\boldsymbol{c_{\mathrm{v}}}$ and $\boldsymbol{c_{\mathrm{d}}}$ are hardening parameters describing how much plastic shear strain, volumetric plastic work and the deviatoric plastic work influence intensity of anisotropy e. They are included in the sensitivity study with variables CA, CV and CD, but with a higher start value than in (Ref 12), since the development of e otherwise is too small.

Explicit values on relevant material constants (and material curves) are summarized in Fig. 1, 2 and Table 1. These values are pertinent to industrially used hard metal powder materials.

3. Cutting Inserts

Four different cutting insert geometries are simulated: three are commercially available and one is more theoretical. They are chosen so that they cover the different stress fields and density variations that may appear in a green body. In an attempt to test the material model and to find new ways for material testing, the theoretical insert is simulated multiaxially, i.e., compacted from different directions.

Insert 1 has a hole that is perpendicular to the compaction direction. Since compaction is symmetric from two sides, three symmetry planes can be assumed; see Fig. 3(a). Insert 2 has a more simple geometry and a hole that is parallel to the compaction direction, shown in Fig. 3(b). The compaction is 30% from the top and 70% from the bottom, and therefore, only two symmetries are assumed. The third insert is compacted in two steps, first 70% in one direction and then 30% in the other, and both compaction directions are perpendicular to the hole as shown in Fig. 3(c). In contrast to the pressing motion, this geometrical shape is simple. The last insert, Insert 4, has a shape that is long and thin, similar to the insert analyzed in (Ref 14), as can be seen in Fig. 3(d).

It should also be mentioned that results for two geometries investigated previously will also be discussed, i.e., the cylindrical die investigated in (Ref 12) and (Ref 13) and also the insert analyzed in (Ref 14) and discussed above.

4. Finite Element Simulations

Finite element simulations are performed quasi-statically in the commercial software LS-DYNA (Ref 15), using explicit

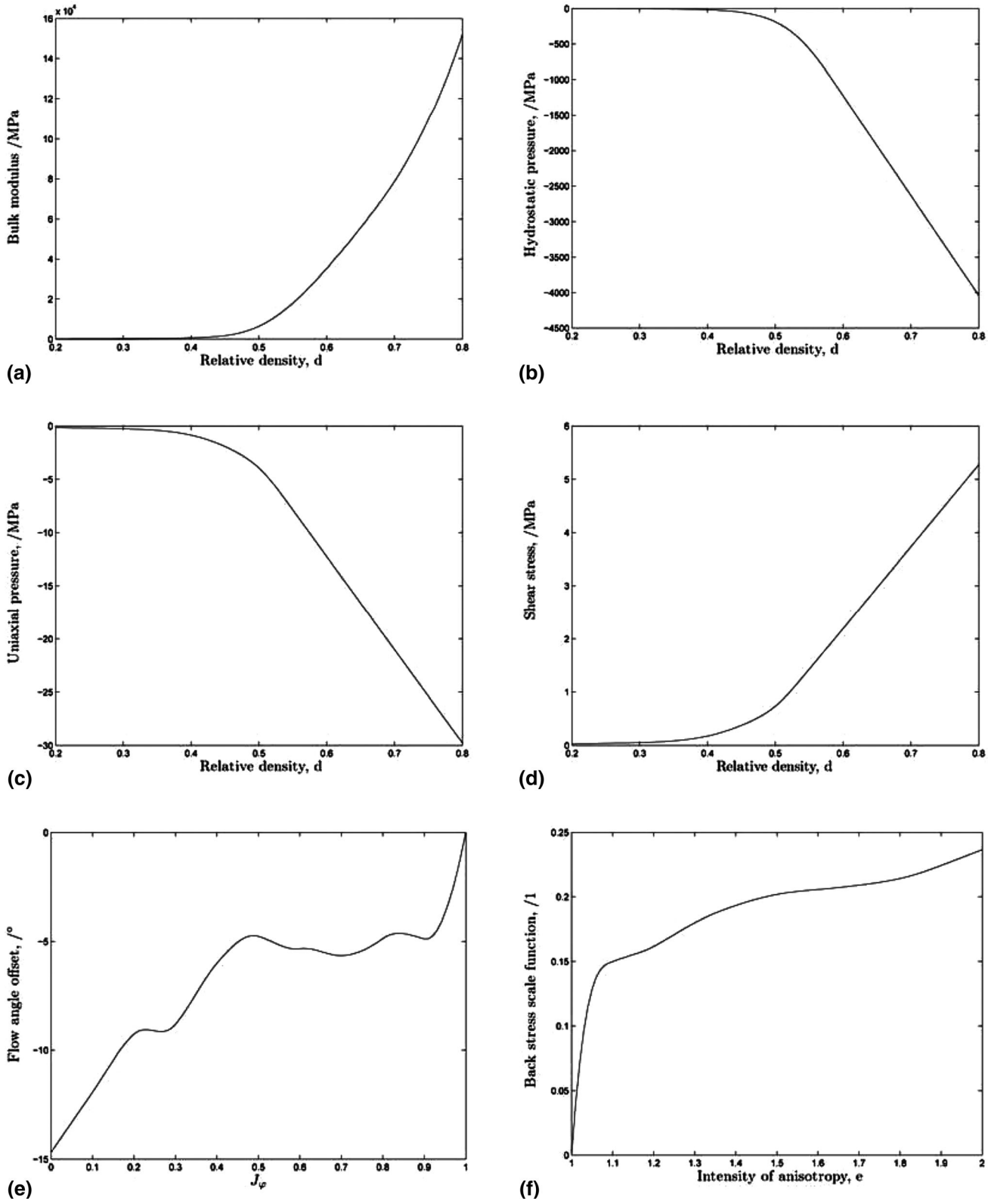

Fig. 2 Material curves suggested in (Ref 11) and used in the analysis scaled. (a) Elastic bulk modulus $K(d)$. (b) Hydrostatic compression yield stress $X(d)$. (c) Uniaxial compression yield stress $Y(d)$. (d) Shear yield stress $C(d)$. (e) Flow angle offset $\varphi(d)$. (f) Back stress scale function $h(d)$

integration. 150,000–250,000 one-point tetrahedron elements that are remeshed during compaction are used to describe the powder. Problems with shear locking are minimized by remeshing. The material model discussed above is implemented in LS-DYNA (Ref 16) and used in all simulations. Pressing tools are assumed to be rigid and modeled with shell elements, and contact is described by the Coulomb friction law, with a frictional coefficient

Table 1 Start, minimum and maximum value for variables included in the sensitivity analysis and how they are linked to material parameters in (Ref 11)

Variables	Material parameter dependence	Notation	Starting	Min	Max
CA	Influence of plastic shear strain on e	c_a	0.0174	0.0148	0.02
CV	Influence of volumetric plastic work on *e*	c_v	0.00087	0.00074	0.001
CD	Influence of deviatoric plastic work on *e*	c_d	0.00087	0.00074	0.001
PR	Poisson's ratio	ν	0.37	0.352	0.389
CFI	Amplitude for offset from flow direction curve	φ(*d*)	0.87	0.74	1
CK	Amplitude for bulk modulus curve	*K*(*d*)	1	0.85	1.15
CC	Amplitude for shear yield curve	*C*(*d*)	0.87	0.74	1
CY	Amplitude for uniaxial compressive yield curve	*Y*(*d*)	1	0.85	1.15
CX	Amplitude for hydrostatic compressive yield curve	*X*(*d*)	1	0.85	1.15
R	Yield surface parameter	*R*	1.14	0.97	1.31
L	Yield surface parameter	*L*	0.85	0.82	0.9

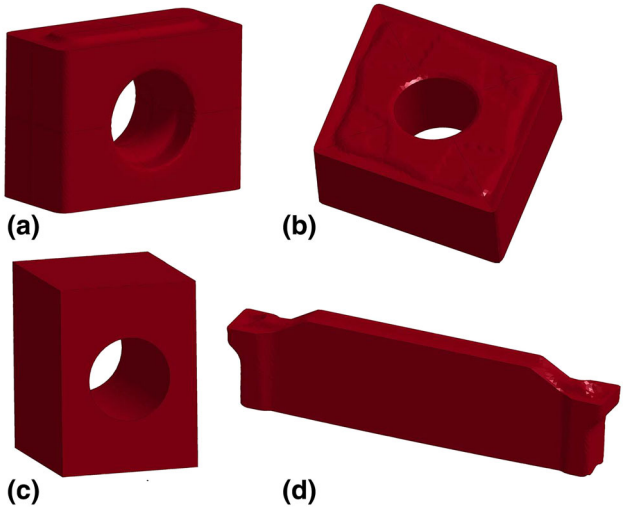

Fig. 3 Shape after compaction (green body) of inserts included in sensitivity studies. (a) Insert 1, cross-hole insert. (b) Insert 2, with hole parallel to compaction direction. (c) Insert 3, compacted multi-axially perpendicular to hole. (d) Insert 4, thin shaped

$$\mu = 0.2, \tag{Eq 8}$$

as thoroughly discussed in (Ref 17).

Figure 4 shows the standard von Mises effective stress

$$\sigma_e = \sqrt{3J_2}, \tag{Eq 9}$$

where J_2 is the second deviatoric stress invariant, at maximum compaction determined from FE-simulations of Insert 1–4 with material parameters from (Ref 12). Figure 5 shows the corresponding results for the relative density *d*, density over sintered density, at maximum compaction. The results in Fig. 4, 5 indicate that the mechanical behavior of the four inserts is quite different and that it is possible to get a fairly complete picture of the properties of the present constitutive description from studying these inserts.

Concerning the accuracy of the present numerical approach, this was investigated in (Ref 1) and (Ref 14), where good agreement was found. In Table 2, maximum pressing forces from FE-simulations and corresponding experiments are compared and also here the agreement is good (Insert 3 is, as described above, a theoretical geometry that is included for completeness and therefore not tested). Accordingly, these results give good confidence in the accuracy of the present numerical approach.

5. Sensitivity Analysis

The material parameters defining the material model described above are included in the sensitivity analysis. Material curves are described with a scale factor, i.e., change in magnitude of material curves is variables in the analysis. For instance, the bulk modulus *K*(*d*), with variable *CK*, is described as:

$$K(d)_{\text{new}} = CK \cdot K(d)_{\text{old}} \tag{Eq 10}$$

Material constants, for example *L*, are simply a variable in the sensitivity analysis. The variables are altered with ±15% in FE-simulations for the sensitivity studies (area of interest). Due to convergence problems in the simulations, some variables have a smaller area of interest, as shown in Table 1.

Each insert geometry is analyzed in a separate sensitivity analysis with two objective functions. One objective function is the von Mises stress σ_e at maximum compaction determined at 10–20 measuring points (sub-objective functions) and the other is relative density *d* determined at the same 10–20 points. The measuring points are distributed over the whole insert and tighter in areas with high stress gradient, as shown in Fig. 6.

The sensitivity analysis is performed by using the commercial software LS-OPT (Ref 18) mainly in two steps. In the first step, FE-simulations with varied material parameters (variables) are performed and used to build a surrogate model (section 2) of each objective function. Since this analysis is only slightly nonlinear in the parameter space and there is some noise due to remeshing, a linear and 150% oversampled Meta model is used. Trials with RBF and quadratic Meta models, as discussed in (Ref 19), show similar results, and therefore, those models would lead to the same conclusions.

In the second step, the Meta model is used to analyze the influence of the different variables linked to material parameters (Table 1). The result is presented by using the Sobol's total effect indices (Ref 20), where zero means that the objective function is completely unaffected by changes of this variable, and a value of one (100%) means that the objective function is

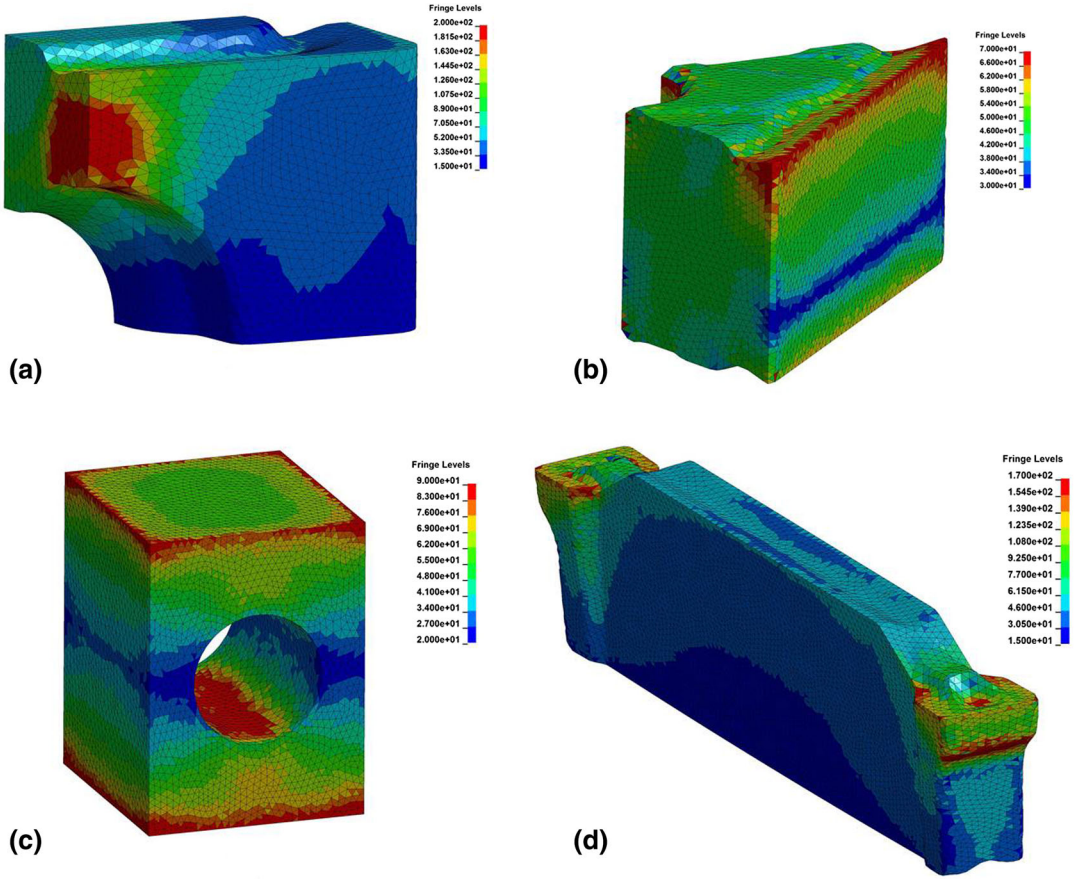

Fig. 4 von Mises effective stress σ_e (MPa) at maximum compaction of Insert 1–4 as described in Fig. 3

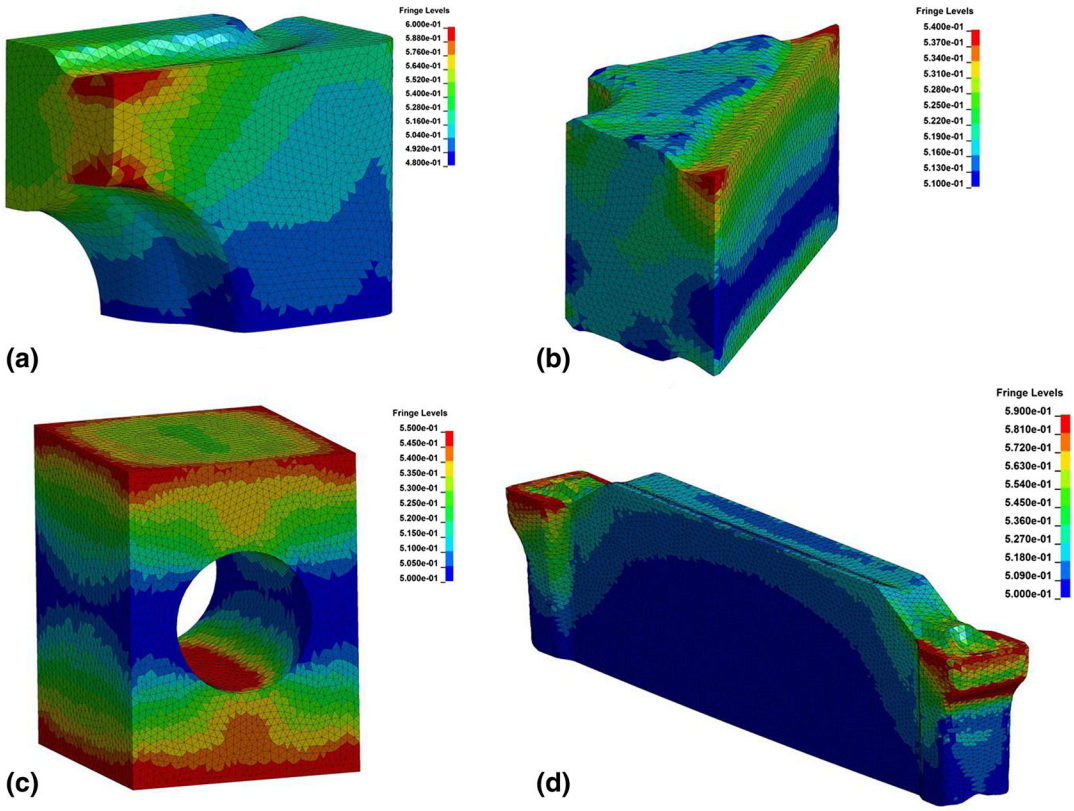

Fig. 5 Relative density *d* (density divided by sintered density) at maximum compaction of Insert 1–4 as described in Fig. 3

dependent only on this variable. The Sobol index is a higher-order sensitivity index, taking into account how variables affect each other, and it should be treated in relative sense within a particular analysis.

Finally in this context, it should be mentioned that error estimation is performed in the sensitivity studies by adding a dummy variable that does not affect the properties in the FE-simulations. In the same manner as for the real variables, the Sobol's total effect index is calculated for the dummy parameter. In the sensitivity studies, the corresponding index, i.e., the error estimation, takes on values between 0.2 and 0.6%, which must be considered satisfactory.

6. Result and Discussion

As mentioned repeatedly, the results discussed below are pertinent to a material parameter sensitivity study based on the constitutive description in the previous section (section 2). All four inserts described in Fig. 3 are included in the sensitivity study, and corresponding results for other types of inserts, presented in (Ref 12-14), are also discussed.

Table 2 Press force at upper punch determined from experiments and finite element simulations

	Experiment (kN)	FE simulation
Press force Insert 1	23	19
Press force Insert 2	24	22
Press force Insert 4	32	32

Insert 3 has not been tested

First of all, however, it seems appropriate to further underline the fact that the mechanical behavior of the cutting inserts studied is different and that it is possible to get a fairly complete picture of the characteristics of the material model by studying these inserts. In doing so, the triaxiality factor, defined as the hydrostatic stress divided by the von Mises effective stress according to

$$\Psi = \frac{p}{\sigma_e} \quad \text{(Eq 11)}$$

where

$$p = \sigma_{ii} \quad \text{(Eq 12)}$$

is determined at maximum compaction; see also (Ref 14). The results are depicted in Fig. 7, and in short, the triaxiality factor differs considerably between the four inserts ensuring completeness of the analysis.

The influence or importance of the different material parameters (and implicitly material curves), with respect to density d and stress σ_e at maximum compaction, is depicted in Fig. 8, 9. The results are pertinent to all the previously discussed inserts (Insert 1–4).

The results indicate that there is a clear difference between the behavior of Insert 1 that has a hole that is perpendicular to the compaction direction, and the rest of the inserts. The relatively large hole in Insert 1 results in large density variation, and since the powder is pushed past the hole also more shearing occurs. This leads to a larger influence from the parameters

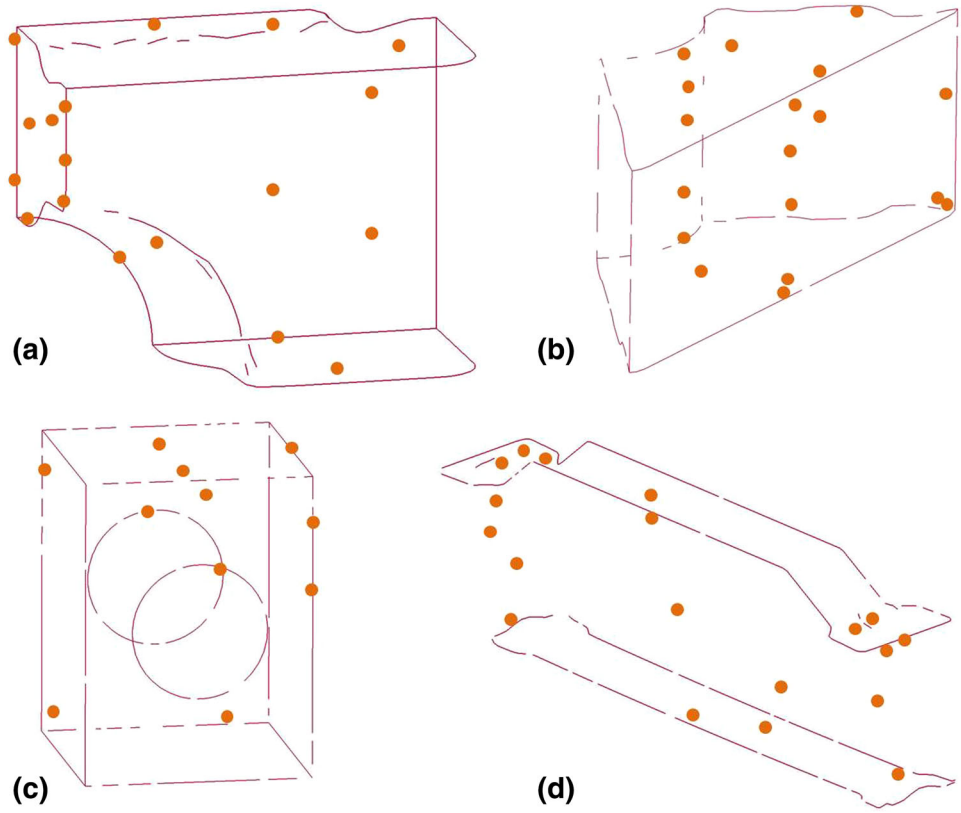

Fig. 6 Points on Insert 1–4 (a–d) where relative density and von Mises effective stress are recorded

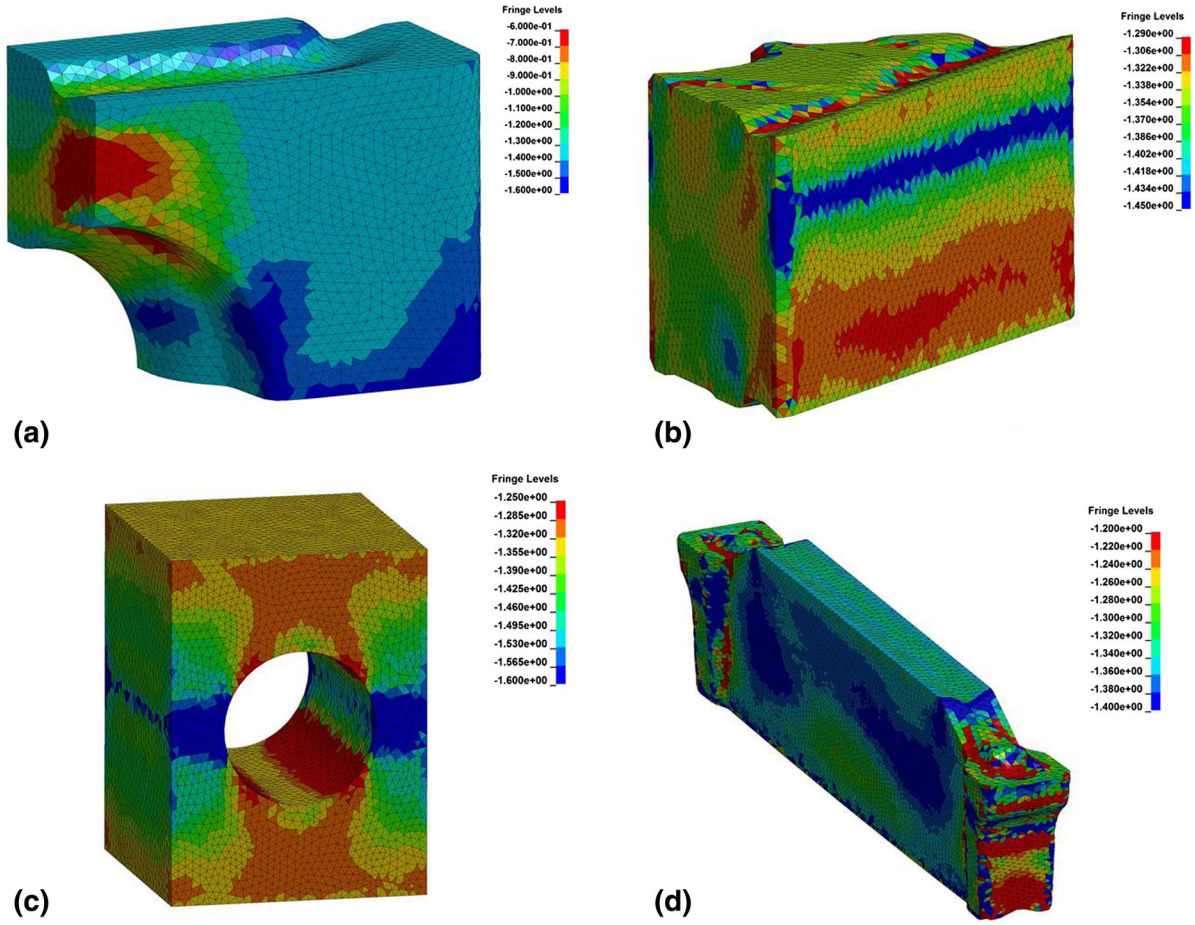

Fig. 7 Triaxiality factor Ψ at maximum compaction of Insert 1–4 as described in Fig. 3

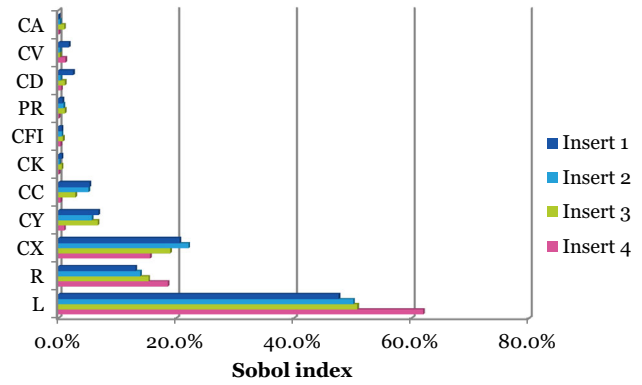

Fig. 8 Influence from variables defined in Table 1, related to the von Mises effective stress σ_e, at maximum compaction of Insert 1–4

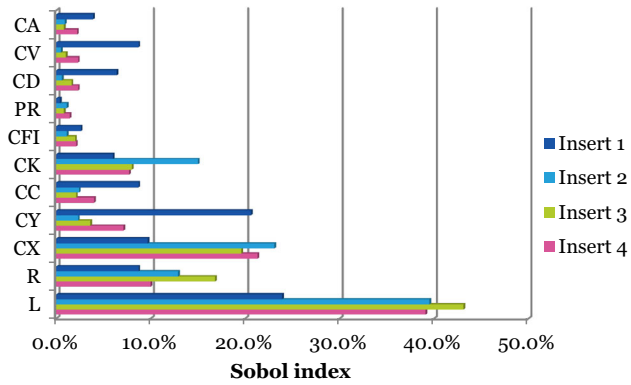

Fig. 9 Influence from variables defined in Table 1, related to the relative density d (density divided by sintered density), at maximum compaction of Insert 1–4

linked to anisotropy (c_a, c_v, c_d), uniaxial compressive yield $Y(d)$ and shearing yield $C(d)$. For the rest of the inserts with a more simple compaction behavior, the hydrostatic compressive yield $X(d)$ is more important and parameters linked to anisotropy have a very small influence.

A corresponding sensitivity analysis studying density and stresses after compaction and unloading was performed and shows similar results as above for density. For the stresses, the elastic parameters Poisson's ratio ν and bulk modulus $K(d)$ are more important, and since unloading is performed in steps with one tool part at the time, the hydrostatic yield curve $X(d)$ is less important, and instead, $Y(d)$, $C(d)$ and $\varphi(d)$ are substantially more influential on the mechanical behavior. These results are not shown explicitly for brevity.

The results from a sensitivity analysis where the force against the wall of an instrumented die is considered, presented in (Ref 12), show that $X(d)$, L and R have a large influence. Concerning the stresses at maximum compaction as analyzed in this paper, the three material parameters with the largest

influence are the same as in (Ref 12). Especially for Insert 4 with a thin shape that in some sense behaves as the instrumented thin cylinder during compaction, the influence from the different parameters is very similar. In this context, it should also be mentioned that the conclusions drawn in (Ref 14) are very close to the corresponding ones from the present sensitivity study pertinent to Insert 4. This is not a surprise though as the insert studied in (Ref 14) resembles Insert 4.

Comparing results for stress with results for density indicates that the influence from the bulk modulus $K(d)$ is more pronounced for density (higher bulk modulus gives more plasticity). The multiaxial compacted insert (Insert 3) shows an even bigger influence from this parameter. This fact is of interest for future material testing as for instance density measurements could be added to inverse modeling complementing the results given by the previously discussed instrumented die.

Finally the results show that for both stress and density the influence from the offset angle function $\varphi(d)$ is small. Since the shape of this function, see Fig. 2, is almost unreasonably complicated, a more simple shape or removing the curve from the material model should be taken into consideration. In this context, it should also be remembered that the offset angle function $\varphi(d)$ is hard to determine experimentally.

The results mentioned above are important for future simplification of the material model, and for future tests that, for instance, could be added to inverse modeling with the instrumented die (Ref 12). As discussed in *Introduction*, the goal is to define a complete set of material parameters for a certain powder blend. Upcoming research will therefore examine the possibility to remove or simplify the offset angle function $\varphi(d)$ and to remove or simplify plastic anisotropy in the material model at issue here. Since the influence from the bulk modulus is more pronounced when looking at the density, density measurements of a green body will also be examined.

7. Conclusions

In the present study, the influence from different material quantities, on the mechanical response at powder compaction, is studied. The material model at issue is an extended Drucker-Prager CAP model, suggested originally by Brandt and Nilsson (Ref 11). The input to the sensitivity study is determined from finite element simulations.

The most important conclusions from this study are:

- Material parameters linked to anisotropy are of small importance for inserts with a simple shape and compaction motion.
- The plastic strain evolution angle $\varphi(d)$ has a small influence on density and stress for all insert shapes.
- The bulk modulus $K(d)$ has a relatively large impact on the density but not on the stress fields.

To define a complete set of material parameters for different powder blends, it is suggested to examine the possibility to remove or simplify the offset angle function $\varphi(d)$ and to remove or simplify anisotropy in the material model, together with further material tests. Since the influence from the bulk modulus is substantial with respect to the density, it is consequently suggested that density measurements of a green body could be added to inverse modeling with the instrumented die.

References

1. J. Brandt, L. Nilsson, Simulating the powder compaction and sintering of cemented carbides with a unified FE-tool. On constitutive modelling of the compaction and sintering of cemented carbides. Linköping studies in science and technology dissertations no. 521, Linköping (1998)
2. B. Storåkers, N. Fleck, and R. McMeeking, The viscoplastic compaction of composite powders, *J. Mech. Phys. Solids*, 1999, **47**(4), p 785–815
3. C.L. Martin and D. Bouvard, Study of the cold compaction of composite powders by the discrete element method, *Acta Mater.*, 2003, **51**, p 373–386
4. E. Olsson and P.-L. Larsson, A numerical analysis of cold powder compaction based on micromechanical experiments, *Powder Technol.*, 2013, **243**, p 1185–1201
5. E. Olsson and P.-L. Larsson, Micromechanical investigation of the fracture behavior of powder materials, *Powder Technol.*, 2015, **286**, p 288–302
6. B. Harthong, J.-F. Jérier, P. Dorémus, D. Imbault, and F.-V. Donzé, Modeling of high density compaction of granular materials by the discrete element method, *Int. J. Solids Struct.*, 2009, **46**(18–19), p 3357–3364
7. B. Harthong, J.-F. Jérier, V. Richefeu, B. Chareyre, P. Dorémus, D. Imbault, and F.-V. Donzé, Contact impingement in packings of elastic-plastic spheres, application to powder compaction, *Int. J. Mech. Sci.*, 2012, **61**(1), p 32–43
8. A.L. Gurson, Yield criteria and flow rules for porous ductile media, continuum theory of ductile rupture by void nucleation and growth Part I, *J. Eng. Mater. Technol. Trans. ASME*, 1977, **1**, p 2–15
9. A. Schofield and C.P. Wroth, *Critical State Soil Mechanics*, McGraw-Hill, New York, 1968
10. F.L. DiMaggio and I.S. Sandler, Material model for granular solids, *J. Eng. Mech. Div. ASCE*, 1971, **96**, p 935–950
11. J. Brandt and L. Nilsson, A constitutive model for compaction of granular media with account for deformation induced anisotropy, *Mech. Cohesive Frict. Mater.*, 1999, **4**, p 391–418
12. D.C. Andersson, P. Lindskog, and P.-L. Larsson, Inverse modeling applied for material characterization of powder materials, *J. Test. Eval.*, 2015, **43**, p 1005–1019
13. P. Lindskog, D.C. Andersson, and P.-L. Larsson, An experimental device for material characterization of powder materials, *J. Test. Eval.*, 2013, **41**(3), p 504–516
14. D.C. Andersson, P. Lindskog, H. Staf, and P.-L. Larsson, On material parameter sensitivity at the production of hard metal components by powder compaction, *J. Mater. Eng. Perform.*, 2014, **23**(6), p 2199–2208
15. J.O. Hallqvist, *LS-Dyna Theory Manual*, LSTC, Livermore, 2006
16. *LS-Dyna Keyword User's Manual II, Material Models* (LSTC, Livemore, 2016), pp. 1278–1284
17. P. Samuelsson and B. Bolin, Experimental studies of frictional behavoir of hard metal powder sliding on cemented carbide walls, *Scand. J. Metall.*, 1983, **12**, p 315–322
18. N. Stander, W. Roux, A. Basudhar, T. Eggleston, T. Goel, and K. Craig, *LS-Opt User's Manual*, LSTC, Livermore, 2014
19. J.H. Holland, *Adaptation in Natural and Artificial Systems*, MIT Press, Cambridge, 1992
20. I.M. Sobol, Sensitivity estimates for nonlinear mathematical models, *Math. Model. Comput. Exp.*, 1993, **4**, p 407–413